# EXPERIMENTAL STUDY OF TWO MECHANICAL DE-ICING SYSTEMS APPLIED ON A WING SECTION TESTED IN AN ICING WIND TUNNEL

M. Endres[1], H. Sommerwerk[2], C. Mendig[3], M. Sinapius[1], P. Horst[2]

[1] Institute of Adaptronics and Function Integration (IAF), Technische Universität Braunschweig, Langer Kamp 6, 38106 Braunschweig, Germany
[2] Institute of Aircraft Design and Lightweight Structures (IFL), Technische Universität Braunschweig, Hermann-Blenk-Str. 35, 38108 Braunschweig, Germany
[3] Institute of Composite Structures and Adaptive Systems, German Aerospace Center (DLR e.V.), Lilienthalplatz 7, 38108 Braunschweig, Germany

**Abstract**

Two mechanical de-icing systems are presented which are applied to a test specimen consisting of a wing section with a NACA0012 profile. The test specimen is of modular design to be able to substitute the leading edge section for investigating the different de-icing and ice detection systems. The de-icing tests are performed in the icing wind tunnel of the Institute of Fluid Mechanics of the TU Braunschweig.
The first de-icing concept is a mechanical system based on structural vibrations of the unstiffened sections. Due to a suitable actuator and its position the skin is excited at its natural frequency. The applied actuators are piezoelectric patch actuators based on the $d_{31}$-effect, which are placed at the inner side of the leading edge.
The second system under investigation is the Electro Impulse De-Icing concept. Coils placed underneath the upper and lower aluminium skin are supplied with short high current impulses which produce opposing time-dependent magnetic fields around coil and skin. The resulting magnetic forces repel the structure which leads to a damped oscillation of the skin.
The first aim of this work is to investigate the performance of the two mechanical de-icing systems under various icing conditions. Operational parameters like temperature and liquid water content are varied in order to attain different ice shapes, ice thicknesses and types of ice (glaze and rime ice). The test results show that the de-icing performance of both systems mainly depends on the ice layer thickness and the environmental temperature. The second aim of this work is to investigate the de-icing mechanism of the ice accumulated on the mechanical de-icing systems. Therefore, the de-icing procedure is recorded with a high speed camera.
The efficiency of both de-icing systems can be increased significantly on a full-scale airfoil, if the ice-covered areas are known. Thus, it is indispensable to have a reliable ice detection system to control the presented de-icing system appropriately.

## NOMENCLATURE

| | | |
|---|---|---|
| LWC | Liquid water content | [g/m$^3$] |
| MVD | Medium volume diameter | [µm] |
| t | Icing time | [min] |
| T | Temperature | [°C] |
| v | Flow velocity | [m/s] |
| α | Angle of attack | [°] |

**Abbrevations**

| | |
|---|---|
| EIDI | Electro Impulse De-Icing |
| FEM | Finite element method |
| FRF | Frequency response function |
| GFRP | Glass fiber reinforced plastic |
| LFDI | Low Frequency De-Icing |

## 1. INTRODUCTION

### BACKGROUND

In flight ice accretion is still a hazard for aviation, especially for aerodynamic surfaces like the airfoil. It causes a decrease in lift and increases the drag, which might lead to an aircraft accident in a worst case scenario. For this purpose ice protection systems are used to protect the critical surfaces.

Nowadays several concepts exist which are already state of the art in aircraft design. Present ice protection concepts can be divided into thermal, mechanical and chemical systems. Bleed air and electro-thermal systems are the most important group of thermal ice protection systems [1], [2]. The bleed air system uses hot pressured air of the turbines which heats up the iced areas while the electro-thermal system uses electrical resistance heat, preferably integrated in the structure. However, two main drawbacks of these systems are the high power consumption and the risk of damaging the composite structure due to the generated heat, if no aditional heat protection is provided.
Chemical systems are based on a porous leading edge, where the de-icing or anti-icing fluid exudes from the surface [3], [4], [5]. The main drawbacks of these systems are the additional weight of the tubes and the de-icing fluid as well as the porous surface which increases the aerodynamic drag of the airfoil.
By contrast, the expectations of mechanical de-icing systems are primarily to reduce the energy consumption compared to the thermal systems and to reduce the overall system weight. Therefore, several concepts have been developed in the last decades. The widest spread system is the pneumatic boots de-icing system, which sheds off the accumulated ice by expanding pneumatic boots placed on the surface of the structure [6], [7], [8].

Another mechanical de-icing concept is the Electro Impulse De-Icing (EIDI) system by which the ice is repelled by electro-mechanical impulses acting on the structure [9], [10]. In addition to these systems, vibration based systems like ultrasonic and low frequency de-icing systems are still on a research stage. With ultrasonic guided waves, accumulated ice can be shed off the surface by exceeding critical shear stresses at the interface [11], [12]. A multitransient actuation showed that the de-iced area can be increased up to 70% compared to continuous driven ultrasonic excitation [13]. However, low frequency systems excite the ice-covered structure with its resonant frequencies to shed off the ice by exceeding critical shear and normal stresses [14], [15], [16]. It can be concluded that all known mechanical systems clearly work as de-icing systems and not as anti-icing systems.

## PAPER OBJECTIVES

The aim of the work is to investigate two mechanical de-icing systems on streamlined profiles with aggregated supercooled water droplets icing, which is one aspect in the project SuLaDI (Supercooled Large Droplet Icing). For this purpose the de-icing systems are tested in an icing wind tunnel under various conditions to compare the results under several aspects. To achieve these goals, the following work steps have to be performed.

1) Design of the de-icing concept for a modular leading edge of the test specimen.
2) Experimental feasibility and de-icing characteristic tests of the systems.
    a. De-icing performance
    b. De-icing mechanism

## 2. MODELLING OF THE DE-ICING TEST SPECIMEN

The structure of the leading edge specimen and the de-icing systems have to be designed. This primarily includes the selection of the actuator and their positions. Especially for the LFDI system the boundary conditions of the test specimen in the test environment are important for the actuator position. Whereas for the EIDI system additional aluminium support, which rigidly positions the coils underneath the leading edge skin is required.
For each de-icing system a particular leading edge is designed, which can be attached to the modular test specimen, depicted in Figure 1.

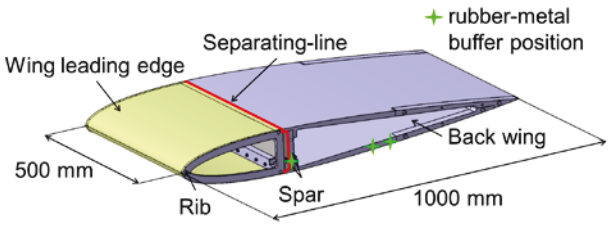


**Figure 1: Modular test specimen for the de-icing tests**

The test specimen is a NACA0012 profile with a total length of 1000 mm. The spars, ribs and the back wing are made out of aluminium alloy.

### 2.1. Low Frequency De-Icing (LFDI)

The first de-icing system is based on actuating resonant frequencies of a wing section, by using piezoelectric patch actuators, placed at the inner side of the leading edge. By applying a voltage, the actuators expand and contract, which leads to a deformation of the surface. At certain frequencies (resonant frequencies) high deformations can be achieved with a small energy input, since the actuator only has to overcome the structural damping. Due to the deformation of the vibrating structure at resonance frequencies, high bending and strain of the skin at the leading edge occur, which leads to ice shedding. The principal functionality and buildup of the leading edge with the de-icing system is depicted in Figure 2. The skin of the leading edge has a thickness of 1 mm and is made of glass fiber reinforced plastic (GFRP).

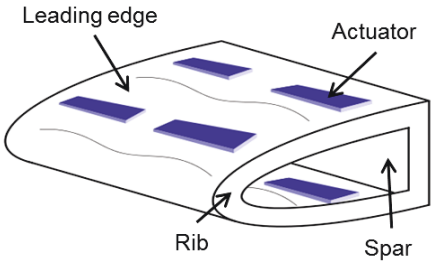


**Figure 2: Schematic view of the Low Frequency De-Icing system (LFDI) on the leading edge**

For a rough approximation of the actuator positions on the leading edge of the test specimen, the boundary conditions of the leading edge skin can be considered as clamping for sufficiently low frequencies. Therefore, a high bending at the peripheral zones of the skin occurs for all eigenmodes. Due to the mechanism of action of the piezoelectric plate actuators and the prevalent boundary condition of the leading edge, the actuator positions are determined near the rib and the spar of the test specimen. For a more precise placement of the actuators, a numerical modal analysis is done with the commercially available finite element tool ANSYS Workbench. It is used to simulate the eigenmodes and the locations with high bending of the leading edge.
Hence, the resonance frequencies of the test specimen are simulated up to 1000 Hz. The resonance frequencies in this frequency band with dominant vibrational amplitudes at the leading edge have a high bending of the skin close to the rib and the spar, as previously assumed.

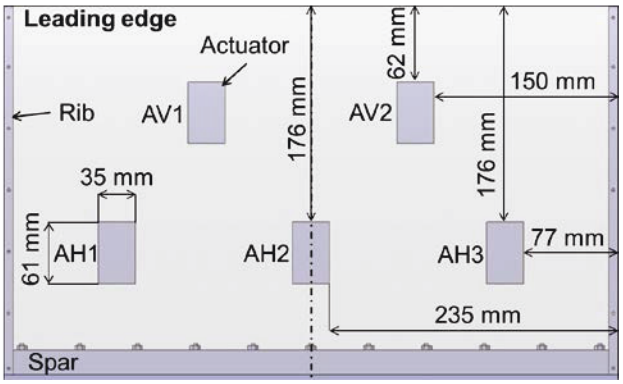


**Figure 3: Actor positions on the upper side of the LFDI leading edge test specimen**

Figure 3 shows the selected actuator positions. In summary ten actuators are placed symmetrically inside the lower and upper side of the leading edge, listed from AH1-AH6 for the actuators close to the spar and AV1-AV4 for the actuators closer to the tip. The actuators AV1-AV4 are placed at this position because of the large number of

different modes with a high bending at this position and to increase the excitation opportunities.

For the actuators, the PI876.A15 piezoelectric patch actuators distributed by PI Ceramic GmbH are selected. They can be excited with a voltage range of -250 V to 1000 V. To avoid any electrical breakdowns a voltage range of -250 V to 750 V is used for the excitation in the experiments.
Previous tests have shown that the lifespan of the actuators significantly decreases due to moisture diffusion into the piezoelectric patch actuators because of the humidity of the test environment. This leads to electrical breakdowns in the actuators. Therefore, a two-component tar-epoxy resin (EP817 FlexShield manufactured by EPIFORM) is used as a coating to prevent moisture diffusion into the piezoelectric patch actuators [17].

### 2.2. Electro Impulse De-Icing (EIDI)

The second de-icing system operates with coils which excite vibrations in the leading edge structure by means of current impulses, cf. [18]. The coils are placed inside the skin with a gap of a few millimeters and fed with short but high impulse currents. The resulting time-dependent magnetic fields cause the structure to oscillate, which can shed off the ice. The schematic structure of the EIDI leading edge is depicted in Figure 4.

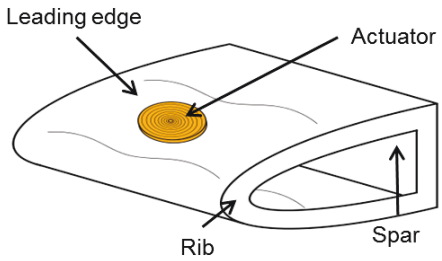


**Figure 4: Schematic view of the Electro Impulse De-Icing system on the leading edge**

Two coils are used, one is positioned to act on the upper part and the other is placed so that it excites the lower part of the airfoil, cf. Figure 5. For the skin a 0.5 mm aluminium foil is used. Due to the small skin thickness, additional circular aluminium doublers are attached to the skin in the coil region. This local gain in skin thickness amplifies the arising magnetic forces so that the required energy for a certain skin deflection is reduced as shown by Zumwalt et al. [9]. The upper and lower coil can be activated by an impulse generator either separately (single coil 1 or single coil 2) or together (coil 1 and 2 in series).

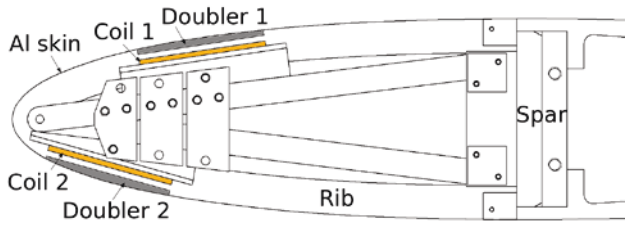


**Figure 5: Coil positions of the Electro Impulse De-Icing leading edge specimen**

## 3. EXPERIMENTAL RESULTS

The tests are performed in the icing wind tunnel of the Institute of Fluid Mechanics of the TU Braunschweig with a test cross section of 500 mm x 500 mm, a flow velocity of 40 m/s and temperatures down to -20°C. By an array of 25 nozzles, the spray bar system achieves a homogeneous droplet distribution with a medium droplet diameter of 90 micrometers. Depending on the adjusted experimental conditions, glaze, rime and mixed ice can be produced.
The experiments are performed with several selected parameter combinations, listed in Table 1.

**Table 1: Icing parameters**

| Icing parameter | Value | Unit |
|---|---|---|
| v | 40 | m/s |
| T | -3 / -10 / -15 / -20 | °C |
| LWC | 1.3 / 2.0 | g/m³ |
| t | 2 / 3 / 4 / 5 / 6 / 8 | min |
| α | 4 / 8 | ° |

The test specimen is installed into the test cross section of the icing wind tunnel mounted with six rubber-metal buffers, depicted in Figure 1, and pressed onto the sidewalls of the test section. Both systems are operated under similar icing conditions.
The variation of temperature is used to achieve different ice types like rime, mixed and glaze ice. Rime ice occurs at lower temperatures and lower LWCs, while glaze ice tends to occur at higher temperatures close to the freezing point and at higher LWCs [19]. Figure 6 shows the ice type results on the GFRP leading edge in the icing wind tunnel at different temperatures.

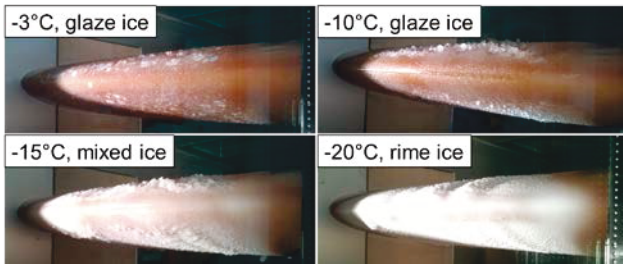


**Figure 6: Accreted ice shapes after 4 minutes of icing on the GFRP leading edge**

For comparing the resulting ice types of the GFRP and the aluminium leading edge, Figure 7 shows different appearances of ice types on the aluminium leading edge. Here, mixed ice already occurs at -10°C and not at -15°C as observed on the GFRP leading edge. This can be explained by the different thermal conductivity of the two leading edge materials. The crystallization enthalpy of the impinging supercooled droplets heats up the environment. Because of the higher heat transfer of the aluminium leading edge, the impingement zones cool down faster after the crystallization of the water droplets which leads to a rime ice formation at higher temperatures compared to the GFRP leading edge.
All presented de-icing tests are performed without any air velocity. Nevertheless, a few tests are carried out with an air flow with different results for the two de-icing systems. A short discussion of the air flow influence is described in chapter 4.

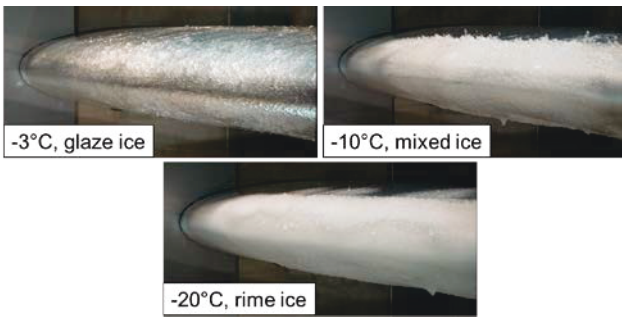


**Figure 7: Accreted ice shapes after 2 minutes of icing on the aluminium leading edge**

### 3.1. De-icing tests of the Low Frequency De-Icing (LFDI)

For the excitation of the actuators the following combination is used for the experiments:

0° phase → AH1, AH2, AH3, AV3, AV4
180° phase → AH4, AH5, AH6, AV1, AV2

A variety of combinations of the actuator excitation is possible and leads to different eigenmodes. Due to the limited test period only the previously listed combination is used. The performance of the de-icing tests is listed in Table 2.

**Table 2: De-icing classification with a sweep excitation at 140 Hz to 950 Hz at 4° angle of attack**

| Temperature \icing time | -3°C | -10°C | -15°C | -20°C |
|---|---|---|---|---|
| 2 min | # | # / + | + / + LWC: 1,3 / 2,2 | + |
| 3 min | | + | | |
| 4 min | # | + | # | -- |
| 5 min | | # | | |
| 6 min | | # | | |
| 8 min | -- | # | | # |

+ (partially de-iced / ice shedding);
# (cracks and delamination, no de-icing);
-- (no cracks, no delamination, no de-icing);

The experiments show that the LFDI system cannot de-ice the leading edge at all testing conditions. Furthermore, in the positive tests the accumulated ice cannot be shed off the surface completely. Two exemplary de-icing results are depicted in Figure 8.
An interesting side effect can be observed during the experiments, depicted in Figure 8. After a certain time, depending on the testing temperature, the accreted ice close to the attached actuators starts to melt due to its heat dissipation. The melted areas are marked with blue ellipses.
The de-iced areas of the leading edge were all covered with a closed ice shape. The areas still covered with ice after the de-icing experiment can be divided into two groups. The first group is characterized by a closed covered ice shape as well, but with a lower ice thickness. These parts are located at the leading edge peripheral areas, close to the rib.
The second group is characterized by partially covered ice shapes. These areas are dominated with feather-shaped ice accumulations and are located chord wise aft of the full covered ice shapes close to the tip of the leading edge.

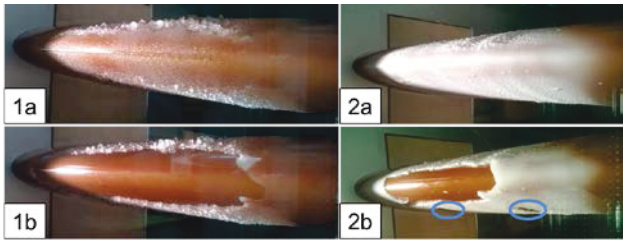


**Figure 8: Ice accretion before (a) and after (b) LFDI de-icing after 4 minutes of icing at -10°C (1a, 1b) and after 2 minutes of icing at -20°C (2a, 2b), 4° angle of attack**

The experiments show that at high temperatures (-3°C) the de-icing system is not able to de-ice the leading edge, and only some cracks occur on the surface. An explanation for this phenomenon could be that at high temperatures, close to the melting point, the delaminated or cracked ice adheres to the surface and refreezes again. Another effect the experiments show is that at temperatures of -15°C and lower, the de-icing system is less effective compared to the de-icing performance at -10°C. An explanation may be the increasing adhesive strength of the ice on surfaces at lower temperatures [20], [21]. Another reason of this effect could be the different types of ice, depicted in Figure 6, and the associated different ice properties.
Another explanatory approach for the de-icing classification of Table 2 is based on the ice thickness of the successful tests. Therefore, the ice thicknesses at the leading edge are listed in Table 3.

**Table 3: Ice thickness at the stagnation line**

| Temperature | -10°C | -15°C | -20°C |
|---|---|---|---|
| Ice thickness after 2 min | ~5 mm | ~6-7 mm | ~4-12 mm |
| Ice thickness after 4 min | ~6-8 mm | - | - |

The consideration of the ice thickness suggests that the de-icing system only works in a particular ice thickness range. This assumption is supported by the effect depicted in Figure 8 for the first group of not de-iced areas. The areas of this group have a lower ice-thickness than the de-iced areas, leading to the result that the de-icing mechanism does not work here. The fact that these areas are close to the supporting ribs can lead to insufficient displacements for the de-icing process.
To explain the areas that cannot be de-iced by the second group, characterized by partially covered feather-shaped ice, the de-icing mechanism has been studied in detail:

## DE-ICING MECHANISM

Because of the mode of action of the system, described in chapter 2.1, high bending and strain appears on the surface. This leads to normal stresses in the ice, tangential to the surface. Furthermore, due to vibration generated inertial forces of the accumulated ice, normal stresses orthogonal to the surface occur. Because of the different material properties of the GFRP and the ice as well as due to the transverse force bending, shear stresses occur at the contact areas. For partially closed ice shapes, like the feather-shaped ice accretion, the critical de-icing stresses cannot be achieved with the

presented test specimen.
For the ice covered areas the superposition of the described mechanism leads to two observed de-icing behaviors in the experiment. These experiments are recorded by a high speed camera with a frame rate of 5000 pictures per second.

The first de-icing behavior is depicted in Figure 9 at a temperature of -20°C and two minutes of icing time. The pictures only show a small section of the leading edge. The excitation is a sweep sinus (140 Hz to 950 Hz). At a certain frequency the delamination of the accumulated ice begins. 0.8 milliseconds later, the ice shape starts to crack at the fringe of the delaminated part. After a second sweep cycle ($t_1$) the delaminated and cracked ice falls off the surface and additional cracks and delamination occur at the fringe. This de-icing phenomenon is the dominant one, which can be observed in all of the recorded experiments.

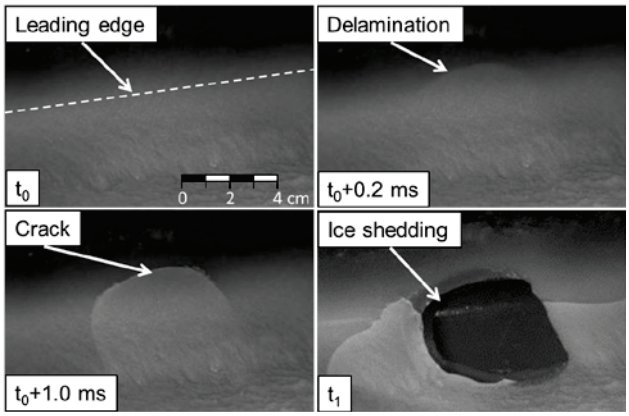


**Figure 9: De-icing mechanism at the leading edge at -20°C and 2 minutes icing time**

The second de-icing behavior is depicted in Figure 10 at a temperature of -10°C and after four minutes of icing. In this case the de-icing mechanism has changed. At first a crack occurs, which leads to a continuously increasing delamination of the accumulated ice. At 6.26 milliseconds the ice has delaminated and after a second sweep cycle, parts of the delaminated ice shed off the surface.

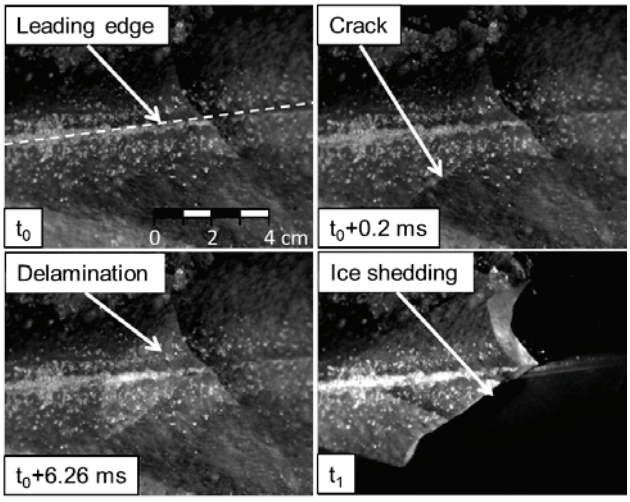


**Figure 10: De-icing mechanism at the leading edge at -10°C and 4 minutes icing time**

## DE-ICING EIGENMODES

The de-icing effect occurs at two different resonance frequencies. The exact frequency cannot be identified due to the sweep excitation and because it differs for each de-icing test due to the different ice shapes, properties and mass. However, a frequency range for the resonance frequencies can be given between 550 Hz and 750 Hz.
The actuator positions do not allow exciting all resonance frequencies occurring in this frequency band. However, an averaged frequency response function (FRF) for the actuator AH1 to the other actuators on the top side (AH2, AH3, AV1, and AV2) of the leading edge gives an overview of the possible frequencies, depicted in Figure 11. The red curves are measured at ~7°C with the test specimen mounted in the icing wind tunnel, fixed with six rubber-metal buffers and pressed onto the sidewalls, while the blue curves are measured in a laboratory at ~20°C with only six rubber-metal buffers fixing the test specimen. The dash-dotted curves are measured after remounting the test specimen. The buffer positions are marked with green stars in Figure 1. The different mounting conditions of the test specimen are caused by the difficulty to retrace the exact conditions in the icing wind tunnel.
The related curves in Figure 11 show a good conformity to each other, especially the curves measured in the laboratory. These curves even show a good correlation for the phase progressions. This can be explained by the good reproducibility of the mounting of the leading edge section and the test specimen. The curves measured in the icing wind tunnel show a greater deviation to each other, caused by the manually tightening of the screws of the sidewalls in the test section of the icing wind tunnel, which presses against the test specimen.
The comparison of the curve progression of the two different mounting types shows a qualitative correlation. Both types show slightly changed but comparable resonance frequencies, exemplarily represented by the two green marked resonance frequencies of the measurement in the laboratory. This means that the different mounting has, as generally known, an effect on the resulting resonance frequencies and eigenmodes, but in this case does not change the eigenmodes in its shape completely.

To identify the de-icing eigenmodes, the recorded de-icing behavior is investigated. Two different types of vibrating modes, which lead to ice shedding, can be identified. These modes are compared with the results of a surface measurement of the leading edge with a scanning vibrometer (PSV-400 from Polytec).
Therefore, the AH1 actuator is selected for a sweep sine excitation from 1 Hz to 1000 Hz at 20 V peak to peak, to identify the excitable eigenmodes of the leading edge. Eigenmodes similar to the recorded (high speed camera) ones in the icing wind tunnel are depicted in Figure 12.
The picture shows the front section of the upper part of the leading edge. An explanation for the de-icing capacity of these modes can be the high amplitudes of closely located peaks and its resulting high bending.

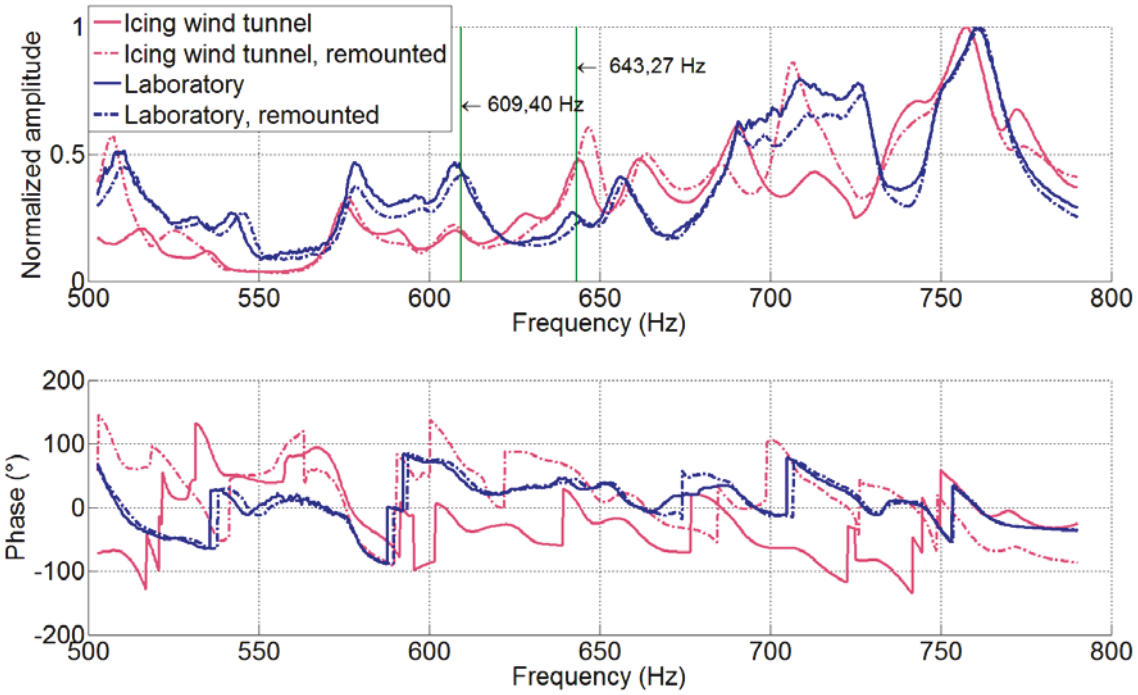


**Figure 11: Comparison of the averaged FRF of the different mounting conditions**

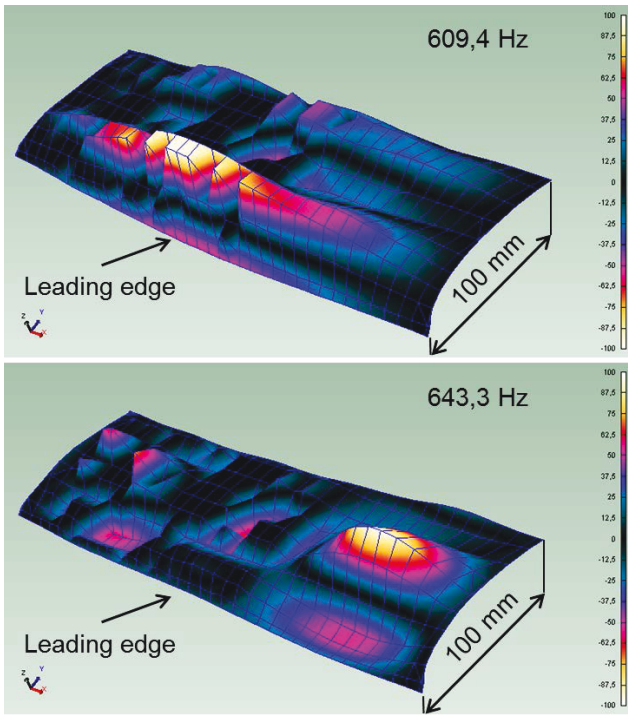


**Figure 12: Two measured eigenmodes with positive de-icing results, on the first 100 mm of the leading edge**

The resonance frequencies measured in the laboratory for the de-iced frequency band with the laser vibrometer are depicted in Table 4. These frequencies differ slightly from the resonance frequencies of the frequency response function of the laboratory measurements, depicted in Figure 11. This difference can be explained by an additional remounting of the test specimen before the scanning vibrometer measurements.

**Table 4: Resonance frequencies measured in the laboratory for the selected frequency band**

| Resonance frequencies (Hz) | Damping (%) |
|---|---|
| 509,50 | 0,63 |
| 534,17 | 0,53 |
| 544,22 | 0,50 |
| 579,41 | 0,55 |
| 599,81 | 0,48 |
| 609,40 | 0,80 |
| 619,83 | 0,34 |
| 643,27 | 0,62 |
| 656,76 | 0,66 |
| 665,41 | 0,49 |
| 693,93 | 0,76 |
| 712,32 | 0,99 |
| 728,91 | 0,57 |
| 750,21 | 0,59 |
| 763,22 | 0,92 |

### 3.2. De-icing tests of the Electro Impulse De-Icing (EIDI)

Each EIDI de-icing trial consists of several de-icing impulses depending on the de-icing performance. Successive impulses are triggered until no further de-icing progress can be noticed. Parameters controlling the de-icing behavior are the coil activation order and the charging voltage. The resulting ice shape determines the activation of either both coils (coil 1 and 2 in series) or of only the lower coil (single coil 2). The charging voltage influences the magnetic field and thus the resulting skin deflection.
First de-icing impulses are generally started at charging voltages which result in a maximum skin deflection of the

clean airfoil of approximately 1.5 to 2.0 mm. In comparison to the resulting maximum deflection of the ice-covered skin, the charging voltage is iteratively increased up to a limit of 2.5 mm deflection within each trial.
The performance of the de-icing tests with the EIDI system is depicted in Table 5. As already mentioned for the LFDI system, a positive de-icing result does not mean that all ice is removed. The structure can be de-iced in most testing cases, only for small ice thicknesses and low temperatures of -20°C the de-icing system shows deficits. The fact that small ice thicknesses are hard to be removed supports the assumption that not only shear stresses in the boundary layer but also cracking processes inside the ice layer influence the de-icing mechanism.

**Table 5: De-icing classification for the EIDI system at 4° angle of attack**

| Temperature \icing time | -3°C | -10°C | -20°C |
|---|---|---|---|
| 2 min | # | + | # |
| 4 min | + | + | # |
| 8 min | + | + | + |

**+** (partially de-iced / ice shedding);
**#** (cracks and delamination, no de-icing);

Figure 13 shows the EIDI leading edge after eight minutes of icing at -10°C and -20 °C before and after de-icing. Similar to the results of the LFDI system, the ice cannot be removed in regions with very small ice thickness or with feather-shaped ice accretion, which arise mainly at -20°C.

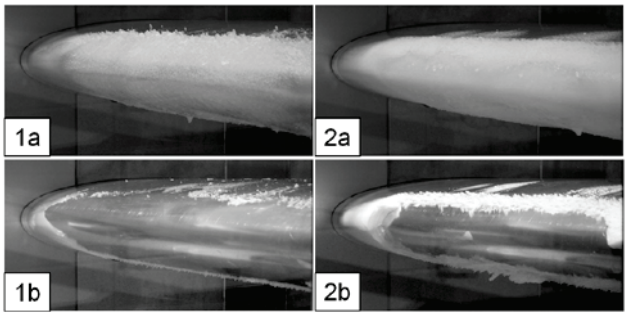


**Figure 13: Ice accretion before (a) and after (b) EIDI de-icing after 8 minutes of icing at -10°C (1a, 1b) and at -20°C (2a, 2b), 4° angle of attack**

## DE-ICING MECHANISM

Similar to the LFDI system, for the EIDI system different de-icing mechanisms, including cracks, delaminations and shedding can be observed. The first impulse generally leads only to cracks and delaminations in the ice layer, whereas shedding occurs in the consecutive impulses.
Close investigations of the first impulses reveal that occasionally the cracks dominate the failure process and at other times delamination occurs prevailingly, as also noticed for the LFDI system.
Figure 14 shows the ice shedding behavior for consecutive EIDI impulses within one de-icing trial. All impulses are triggered with the same charging voltage. In the beginning attempts are made to de-ice the leading edge by activation of both coils in series. Since ice accretion occurs due to the high angle of attack mainly on the lower part of the airfoil, activation of only the lower coil (coil 2) proves to be more beneficial. Whereas the impulses with coil 1 and 2 in series only cause some cracks in the ice layer, impulses with only coil 2 achieve to shed off the ice progressively. After the sixth impulse most of the accreted ice is removed, besides some ice in the doubler region and in the boundary regions close to the ribs. The latter one cannot be removed due to the small ice thickness, as mentioned before. The ice segment in the doubler region remains on the structure due to the increased stiffness in this area.

## 4. COMPARISON AND CONCLUSION

Both mechanical de-icing systems presented in this work achieve successful de-icing results with different limitations. The best results are obtained at -10°C for both systems. For higher temperatures (-3°C) the accreted ice tends to refreeze at the delaminated or cracked areas after the excitation of the systems. At lower temperatures (-20°C) the increasing adhesive strength of the accreted ice impedes the ice shedding. In addition, both systems lack the ability to de-ice the thin ice layers close the rib at the leading edge and the feather-shaped areas closer to the spar in case of the current test specimen design. This means that the achieved strains and stresses in the contact layer of the ice and the skin are not high enough to overcome the critical de-icing values.
Apart from that the experiments also show some differences concerning the de-icing feasibility. The LFDI system tends to a better performance for thin ice layers after two minutes of icing than the EIDI system. However, the ice layer in the region of the aluminium doubler does not shed off the surface.

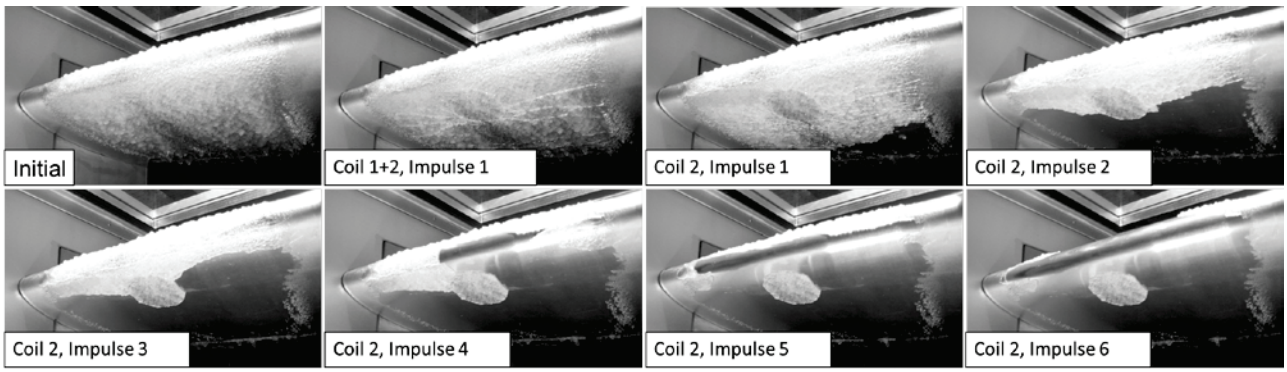


**Figure 14: Shedding behavior for consecutive EIDI impulses, at -3°C, 8° angle of attack and 4 min icing time**

.

This is substantiated by the fact that this area provides a higher stiffness leading to lower local bending and lower relative displacements. In contrast, the LFDI system melts the ice underneath the patch due to thermal dissipation of the excitation. Especially for thermal sensitive materials like CFRP and GFRP, the heat emission of the actuators has to be observed to protect the structure.
The de-icing mechanism is similar for both presented de-icing systems. Two different behaviors can be observed during the experiments. The prevailingly occurring behavior is a cracking of the ice caused by previous delamination of the affected ice layer. Occasionally the failure process switches to delamination, resulting from cracks in the ice layer.
A few feasibility tests are performed with an airflow velocity of 40 m/s. The de-icing performance of the EIDI system can be improved in these tests. The cracked and delaminated ice patches rather tend to shed off the surface due to the airflow. In contrast, the LFDI system shows the opposite behavior. The airflow presses the ice patches against the skin of the leading edge, whereby no de-icing is recorded. After the airflow turns off, with present excitation, the ice patches shed off the surface. A possible explanation for this behavior may be the actuation type. While the EIDI system gives a short impulse, which leads to a high deformation and deformation velocity, the LFDI excites the structure with harmonic excitation. Since only one test with the LFDI system and three tests with the EIDI systems are performed with airflow, a generally statement cannot be made for the observed behavior.

Finally, the question arises which de-icing effect should be targeted by mechanical de-icing systems. The ultrasonic systems try to reach the critical shear stresses of the accreted ice, which leads to a shearing delamination process, whereas with a single frequency excitation at a structural resonance frequency the normal stresses on the unstiffened areas should be dominant, which leads to a peeling effect of the ice. In conclusion both, shear and normal stresses, lead to de-icing of the accumulated ice. It is a superposition of both effects whose influences depend on the mechanical de-icing system and its type of excitation.

Since both system show successful de-icing results for the closed ice layers, but lack the ability to de-ice thin peripheral ice layers and the feather-shaped accreted ice, some possible improvements should be mentioned.
The LFDI system could be improved by different excitation combinations of the actuator. Different eigenmodes could lead to different de-icing behaviors. In addition, a controlled excitation of the actuators could improve the de-icing effectivity enormously, since no inappropriate frequencies are excited. Controlling the excitation and the structural response enables tracing of resonance frequencies and prevents idle times during the de-icing. Excitation beyond the resonance frequencies leads to much lower amplitudes associated with insufficient stresses.
Concerning the EIDI system, different coil positions can be examined. Furthermore, the number of coils can be increased to study the interaction of several coils.

Regardless of the mechanical de-icing system, the efficiency can most likely be improved if an additional thermal system is integrated into the structure. Thus, the mechanical de-icing can remove as much ice as possible in the first place, whereas the energy consuming thermal system is only applied if necessary.
Enlargements on a full scale wing enable further possibilities to improve the system efficiency, for example with local ice detection systems placed span-wise on the leading edge of the airfoil. With such an ice detection system the iced and ice free areas could be identified and only the actuators located at the iced parts have to be excited, which leads to a lower energy consumption.
Since the accumulated ice on the leading edge has an influence on its resonance frequencies related with the eigenmodes, the frequency response function of the actuators could also be used as an ice detection criteria. In Addition, the actuators can be used for ice detection via ultrasonic through the excitation of guided waves as mentioned for example in [22].

## 5. ACKNOWLEDGMENTS

The authors would like to acknowledge the support of the Institute of Fluid Mechanics of the TU Braunschweig Icing Wind Tunnel staff.

## 6. REFERENCES

[1] A. D. Shah, *Integrated Thermal Anti-Icing and Environmental Control,* English. 535,928, 1976.
[2] G. C. Botura, D. Sweet and D. Flosdorf, *Development and Demonstration of Low Power Electrothermal De-icing System,* Reno, NV: 43rd AIAA Aerospace Sciences Meeting and Exhibition, Jan. 2005. DOI: 10.2514/6.2005-1460
[3] D. Kohlman, W. Schweikhard and P. Evanich, *Icing Tunnel Tests of a Glycol-Exuding Porous Leading Edge Ice Protection System,* Journal of Aircraft, 1982, pp. 647--654. DOI: 10.2514/3.57445
[4] A. Heinrich, R. Ross, G. Zumwalt, J. Provorse, V. Padmanabhan, J. Thompson and J. Riley, *Section 3.0 Fluid Ice Protection Systems,* U. S. Department of Transportation, FAA, 1991.
[5] A. Albright, *A Summary of NASA's Research on the Fluid Ice Protection System,* 23rd Aerospace Sciences Meeting ed., Reno, Nevada, AIAA, 1985.
[6] A. Heinrich, R. Ross, G. Zumwalt, J. Provorse, V. Padmanabhan, J. Thompson and J. Riley, *Section 1.0 Conventional Pneumatic Boot Deicing Systems,* U. S. Department of Transportation, FAA, 1991.
[7] J. Shin, T. H. Bond und G. A. Mesander, *Results of a Low Power Ice Protection System Test and a New Method of Imaging Data Analysis,* National Aeronautics and Space Administration, 1992.
[8] D. Sweet, *Understanding pneumatic de-icing,* Goodrich, 2011.
[9] G. W. Zumwalt, R. L. Schrag, W.D. Bernhart and R. A. Friedberg, *Electro-Impulse De-Icing Testing Analysis and Design*, NASA CR-4175, NASA, USA, 1988.
[10] R. A. Henderson and R. L. Schrag, *Theoretical Analysis of Electrical Aspects of the Basic Electro-Impulse Problem in Aircraft De-Icing Applications*, NASA CR-180845, NASA, USA, 1987.
[11] Y. Zhu, J. L. Palacios, J. L. Rose and E. C. Smith, *De-icing of Multi-layer Composite Plates Using Ultrasonic Guided Waves,* Proceedings of the 49th Structural Dynamics and Materials Conference, 2008. DOI: 10.2514/6.2008-1862
[12] J. Palacios, E. Smith and J. Rose, *Instantaneous De-Icing of Freezer Ice via Ultrasonic Actuation,* 49 ed.,

AIAA Journal, 2011, pp. 1158--1167. DOI: 10.2514/1.J050143

[13] N. DiPlacido, J. Soltis and J. Palacios, *Enhancement of Ultrasonic De-Icing via Tone Burst Excitation,* Journal of Aircraft, 2016. DOI: 10.2514/1.C033761

[14] S. V. Venna, Y.-J. Lin and G. Botura, *Piezoelectric Transducer Actuated Leading Edge De-Icing with Simultaneous Shear and Impulse Forces,* Journal of Aircraft, 2007. DOI: 10.2514/1.23996

[15] H. Habibi, G. Edwards, L. Cheng and H. Zheng et al., *Developing a Novel Ice Protection System for Wind Turbine,* SAE International, 2015. DOI: 10.4271/2015-01-2081

[16] E. Villeneuve, D. Harvey, D. Zimcik, R. Aubert, J. Perron, *Piezoelectric De-icing System for Rotorcraft,* Journal of the American Helicopter Society, 2015. DOI: 10.4050/JAHS.60.042001

[17] C. Behr, F. Lippmann, P. Wierach, M. Sinapius, *Tailored Multilayer Stack Actuators for Harsh Environment*, 7th ECCOMAS Thematic Conference on Smart Structures and Materials, 2015

[18] H. Sommerwerk, P. Horst and S. Bansmer, *Studies on Electro Impulse De-Icing of a Leading Edge Structure in an Icing Wind Tunnel*, 8th AIAA Atmospheric and Space Environments Conference, Washington, D.C., June 2016. DOI: 10.2514/6.2016-3441.

[19] R.W. Gent, N. P. Dart, J. T. Cansdale, *Aircraft Icing,* Philosophical Transactions of the Royal Society A 358.1776, P. 2873–2911, 2000. DOI: 10.1098/rsta.2000.0689

[20] H. H. G. Jellinek, *Adhesive Properties of Ice,* Journal of Colloid Science 14.3 (1959), S. 268–280. DOI: 10.1016/0095-8522(59)90051-0.

[21] W. Dong, J. Ding und Z. X. Zhou, *Experimental Study on the Ice Freezing Adhesive Characteristics of Metal Surfaces,* Journal of Aircraft 51.3 (2014), S. 719–726. DOI: 10.2514/1.C032393.

[22] Huidong Gao, Joseph L. Rose, *Ice Detection and Classification on an Aircraft Wing with Ultrasonic Shear Horizontal Guided Waves*, IEEE Transactions on Ultrasonics, Ferroelectrics, and Frequency Control, vol. 56, no. 2, February 2009, S. 334-344. DOI: 10.1109/TUFFC.2009.1042